RESEARCH PAPER

Geospatial Data Extraction from Satellite Imagery for Road Construction Planning and Monitoring

Yash Mahendra Ramteke[1], Sudhanshu Pathak[1], Rohit Jadhav[2], Smita Pataskar[1], Sachin Mane[1], Shubham Chandgude[3]

[1]Department of Civil Engineering, D. Y. Patil College of Engineering, Akurdi, Pune, Maharashtra, India

[2]Department of Robotics and Automation, D. Y. Patil College of Engineering, Akurdi, Pune, Maharashtra, India

[3]Department of Civil Engineering, D. Y. Patil International University Akurdi, Pune, Maharashtra, India

ABSTRACT

Conventional road survey methods such as Total Station and Differential GPS (DGPS) are accurate but time-consuming, labour-intensive and spatially-limited. Thus, they are unsuitable for large-scale or rapid monitoring of infrastructure. This study speaks for the need of a scalable, affordable alternative.

Using state-of-the-art satellite imagery, computer software was developed in Matlab and GIS for achieving a semi-automated structured methodology. The workflow involved taking images, geo-referencing them, converting to grayscale, noise reduction through filtering with a median filter, Canny edge detection for road boundary detection, a morphological operation by skeletonizing to extract the centreline, and finally calculating the width and length of the road programmatically. Road type classification was done using Indian Road Congress (IRC) width standards.

Findings: The methodology was validated against DGPS ground-truth data for straight and curved road stretches. Accuracies of the extracted parameters were 90% for both segment types. For straight road, length was 270.12 m (accuracy: 90.00%), width was 10.90 m (90.08%). For curved road, arc length was 90.00 m (90.91%), width was 12.00 m (90.91%).

To conclude, the satellite imagery-based approach is feasible, reliable, repeatable, and cost-effective tool that can supplement or replace traditional surveys. Further, this method may be implemented directly in the construction planning phase for material estimation, computation of earthworks volume, project planning, and scheduling.

Keywords: Satellite Imagery; Road Classification; Construction Progress Monitoring; Image Processing; MATLAB; Remote Sensing; GIS; Canny Edge Detection.

How to cite this article: Ramteke Y M, Pathak S, Jadhav R, Pataskar S, Mane S, Chandgude S. Geospatial Data 2026;16(67s):1966-1990. DOI: 10.25258/ijddt.16.67s.177

Source of support: Nil

Conflict of interest: None

1. INTRODUCTION

The second-largest road network of the world is in India which covers 6.37 million kilometres (MoRTH, 2023). The Indian Roads Congress (IRC) has fixed the design provisions for the four-level network which consists of National Highways, State Highways, Major District and Other District Roads and Village Roads. Geospatial information is crucial information for every phase of the project starting from alignment planning and earthwork design during the active construction and long-term condition monitoring. The parameters of the carriageway's width, the segment's length, the horizontal curvature and the pavement's condition feed into the quantities, costs and schedules of the works directly [1].

The recent commitment of national programs like Bharatmala Pariyojana, Smart Cities Mission and Pradhan Mantri Gram Sadak Yojana (PMGSY) of several lakh crore rupees for the construction and rehabilitation of roads. The use of traditional instruments to handle geospatial information for such long networks is not a good use of either time or money. In India, the Twelfth Five-Year Plan, designated geospatial technology as a strategic lever for infrastructure oversight. That was reiterated in the following policies [2].

On the whole ground-based survey instruments like Total Station (TS), Differential GPS (DGPS), Electronic Distance Measurement (EDM), Mobile LiDAR Systems (MLS), and terrestrial laser scanners (TLS) give one centimeter-class positional accuracy. On a network scale applicability, however, they have four basic limitations.

It is time-consuming, requires a huge workforce and involves high equipment costs to mobilise for large-area campaigns. The fixed mobilisation and staffing costs make it unaffordable for smaller or rural projects. The temporal gap between campaigns allows changes in construction to go undetected. Inaccessibility due to rugged terrain or security-sensitive areas may lead to partial or complete surveys not being carried out. Given all of this, exploring scalable remote-sensing alternatives becomes attractive

The operational availability of very-high-resolution (VHR) commercial satellite imagery, inaugurated by IKONOS (1999) and now extending to WorldView-3 (0.31 m GSD), GeoEye-1 (0.41 m GSD), Pleiades-1 (0.50 m GSD), and the Indian Cartosat-3 (0.25 m GSD), has transformed what is achievable from orbital platforms. With sufficient pixel density, the carriageway boundaries are resolved at a sub metre ground sampling distance. Thus, it permits the extraction of geometric parameters to engineering accuracy levels. Aggregated imagery like Google Earth Pro is available free of charge, which further reduces the entry barrier for research and preliminary planning application [4].

The image processing toolbox of MATLAB is a transparent, script-level environment in which every processing decision is evident and audit-able. This creating auditable versioned workflow has great benefit in engineering applications where reproducibility of the workflow and regulatory traceability.

MATLAB-based classical pipelines work on normal workstation hardware without needing any specialist machine-learning expertise, unlike end-to-end deep learning frameworks which require GPU infrastructure and large annotated training corpora. As such, the method can be made available to the broader civil engineering community in low resource settings around the developing world [5].

Bringing satellite remote sensing into project management sees a conceptual shift in thinking from measurable point sampled field data to the spatially continuous time-repeatable monitoring. Outputs that are compatible with Building Information Modelling (BIM) environments, GIS project management platforms, and quantity-surveying tools provide a digital chain that extends from satellite observation to procurement action. This study illustrates this chain in quantitative detail.

The study proposes a semi-automated workflow using GIS and MATLAB to evaluate road characteristics from high-resolution satellite imagery. A minimum accuracy threshold of 85 per cent of DGPS ground truth was targeted to validate the workflow.

The flow of the paper is as follows: The problem statement is framed in Section 2; research objectives are stated in Section 3; the study area is described in Section 4; related literature is reviewed in Section 5; methodology and mathematical formulations are determined in Section 6; results are presented in Section 7; findings and limitations are discussed in Section 8 and conclusion and future directions are drawn in Section 9.

2. PROBLEM STATEMENT

In India, modern road engineering requires more data than traditional surveys, resulting in an increasing technology gap due to the standard survey output limitation. Efforts being undertaken to upgrade ground truthing of national highway schemes that are under implementation especially at the execution stage need to be complemented with effective capacity building specifically for all DGPS traverse component surveys and to ensure that all infrastructures and equipment are in place for the same.

The problem has three structural constraints. The time limitation is because a DGPS campaign of 10 km road corridor needs 3 to 5 field days under normal condition which means the project wise data is always lags by few weeks behind the construction front so that the geometric deviation from the approved drawing may get worsen before getting caught.[2] One of the sources of compounding uncertainty in quantity calculations for the road with variable cross-section is inter-station geometry, which is inferred, and not observed. This spatial constraint has its origin in the station-interval nature of ground surveys, namely, taking cross-sections of road works every 20-50 m for earthworks and every 5-10 m for pavement. The accessibility constraint is wherever flooding from monsoon season, tough terrain, or security issues render physical survey impossible, resulting in data gaps causing distortion in project monitoring records.

Researchers have created algorithms capable of extraction of roads – U-net, Segnet, various DeepLab making use of neural networks type of architectures. And these report Intersection-Oover-Union measures over 0.85 in use on data from benchmarks like SpaceNet, DeepGlobe. The aggregate of this research underwhelms in fulfilling civil engineering needs in four ways; most methods classify pixels as road or non-road as opposed to measuring carriageway size in metres. Training deep networks require large labelled datasets which are expensive to assemble for site-specific Indian contexts. Neuronal network outputs resist the interpretability and auditability for compliance documentation. GPU-dependent inference pipelines also lie outside the 'standard software environment' of practising engineers [3, 4].

Many studies that do report dimensional accuracy against ground control are based on North American or European road networks; these studies are often reliant on design standards, pavement materials and urban morphology of a different class from the Indian IRC. There has not yet been any development of an end-to-end pipeline that (a) extracts width, length, and type from satellite imagery in the Indian urban context, (b) validates it against DGPS ground truth, (c) maps it to the IRC road-classification system, and (d) converts the extracted parameters into construction planning quantities.

The absence of a pipeline that translates imagery and DEM data directly into construction-level outputs inspired the current research. This study fills that gap by putting forth a transparent MATLAB-based pipeline requiring no training data and no GPU hardware against DGPS-surveyed road segments in Akurdi, Pune. The pipeline is shown to translate imagery and DEM data into bill-of-quantities outputs and GIS-ready shape files.

3. OBJECTIVES

This research study has specific objectives.

1. To aims at creating a semi-automated image processing pipeline in MATLAB for the extraction of road parameters such as road width, road length, and type from satellite imagery.
2. To categorize the types of roads based on the derived values of their widths as per IRC design standards.
3. The goal is to validate satellite-derived road parameters against high-precision DGPS ground-truth measurements of both straight and curved road segments.
4. To show directly applying parameters extracted to construction planning like paving area estimation, material volume computation and GIS shapefile creation for project use.
5. To evaluate the potential of the proposed methodology as an economical and scalable alternative or supplement to conventional field survey methods for road infrastructure monitoring in India.

4. STUDY AREA

4.1 Geographic location and administrative setting.

The study is focused on Akurdi, a region under the Pune Metropolitan Region (PMR) within the Pimpri-Chinchwad Municipal Corporation (PCMC) of Maharashtra, India. The geographical center of the research area is situated in the eastern Deccan Plateau physiographic zone. Its WGS-84 coordinates are approximately 18.647°N, 73.770°E. Administering more than 1,500 km of classified roads in their jurisdiction, PCMC is amongst the most road-dense municipal councils in India. The location of the study is approximately 3.5 km north of Pimpri railway station, and it has access to NH-48 (Mumbai–Pune corridor) with Nashik Phata interchange [1].

4.2 Characteristics of the analysed road segments.

Two different stretches of road were chosen for the analysis. Segment S-R001 serves as a north–south arterial road along D's frontage. Y. Approximately 300 m long, a two-lane divided carriageway. As per the DGPS measurements, the mean carriageway width has been found to be 12.10 m with 2.0 m central median and 1.0 m shoulders on either side, which conform to IRC:86-1983 (Geometric Design for Urban Road in Plains). According to IRC: 37-2018, Dense Bituminous Macadam is used for the wearing course, and the subgrade comprises black cotton soil over weathered Deccan Basalt.

Figure 1. Location map of the study area in Akurdi, Pune (18.647°N, 73.770°E), showing the positions of Segment S-R001 (straight arterial) and Segment C-R001 (curved collector junction). Base map: Google Earth Pro (imagery date: post-monsoon 2023). Scale bar and north arrow shown.

Segment C-R001 of the DTT Project is a secondary collector road forming a T-junction approximately at an angle of 45° with S-R001. The DGPS survey verified its arc range of 99.00 m and carriageway width of 13.20 m. Both areas show features that are characteristic of Indian urban arterial areas, such as patchy canopy cover which results in partial occlusion of the satellite image, varied pavement condition ranging from newly surfaced areas to heavily patched areas, boundary interruptions caused by street furniture and parked vehicles, and visible or partially visible centre-line and edge-line markings which can potentially be used as reference features during validation.

4.3 Specification for Satellite Imagery

Imagery for both areas was acquired from Google Earth Pro (version 7.3.6), which merges acquisitions from a range of VHR commercial platforms – predominantly WorldView-2/3 (Maxar Technologies) and GeoEye-1. Through empirical scale calibration, it was determined that the Ground Sampling Distance (GSD) was approximately 0.4668 m/pixel for the S-R001 scene (Low zoom) and 0.1471 m/pixel for the C-R001 scene (High zoom). The values in question match the ones in WorldView-2 panchromatic imagery with 0.46 m GSD [3]. The imagery in all the cases were taken under favourable situation and includes clear sky; solar zenith angle of 30 to 40 from nadir (typical of Pune in post-monsoon winter months); no cloud cover; trace atmospheric haze. The red-green-blue (RGB) composite gives three spectral channels, namely, 630–690 nm (red), 510–580 nm (green), and 450–510 nm (blue).

These provide adequate luminance-contrast for road marking delineation.

Figure 2. Satellite images of study area-Akurdi, Pune on Google Earth Pro. The above-mentioned north–south arterial road corridor (Segment S-R001, ~300 m) is highlighted in yellow; the curvature junction approach (Segment C-R001, ~99 m arc) is highlighted in cyan. Imagery GSD: ~0.47m/pixel. The top is north. Source: Google Earth Pro/Maxar Technologies.

4.4 DGPS Survey on the Ground Truth

The Trimble R8 GNSS receiver used in RTK differential mode helped in getting ground-truth measurements with a horizontal position accuracy of ± (8 mm + 1 ppm). The base station RTK was set up at PCMC Survey Mark PN-2847, a benchmark point verified against the SOI trigonometric network. The rover made observations at station intervals of 5 m along both segments with triple-epoch occupations; the PDOP stayed below 2.5 for the duration of each campaign giving ±12 mm (1σ) positional repeatability (4). The width of the carriageway was measured at cross-section intervals of 10 m using a calibrated fibreglass tape. 31 cross-sections were recorded for S-R001 (mean 12.10 m) and 12 for C-R001 (mean 13.20 m). The total arc length has been calculated as the sum of chord lengths between consecutive DGPS stations, 300.13 m for S-R001 and 99.00 m for C-R001.

4.5 Reason for Site Selection.

Based on five criteria acting in combination, Akurdi was chosen. First, sub-metre Google Earth Pro imagery is available for the site with documented acquisition metadata, thus ensuring study reproducibility. Second, the coexistence of both linear and curved road segments within a tight area allows the evaluation of the algorithm at two geometrically distinct scenarios without any issue of logistics. Third, institutional proximity to provided direct physical access for the DGPS survey. Moreover, the road typology, pavement material and urban context of the site are broadly representative of Tier-1 and Tier-2 Indian cities. Therefore, this supports the generalisation. The GSD ~0.47m ensures that the 12-13m carriageway widths subtend ~26-28 pixels which is comfortably above the ~12-pixel minimum required for reliable edge localisation.

5. LITERATURE REVIEW / RELATED WORK

5.1 Historical evolution of extracting roads from imagery.

From the early 1990s onward, systematic research began on the automated road feature extraction from remotely sensed imagery. Grün and Li (1995) were some of the first to formalise road centreline detection as an optimization problem using dynamic programming on aerial photography. Subsequent enhancements took place following improvements in satellite resolution and computing.

Mena and Malpica [12] proposed a two-layer technique based on multispectral thresholding (MST) and morphological filtering (MF) for road extraction in rural and peri-urban VHR images. This is among the early contributions to the spectral-morphological tradition. In open scenery they do a good job but their performance degrades in occlusion heavy scenes usually found in urban areas. In continuation of this work, Mokhtarzade and Zoej proposed a pipeline of grayscale thresholding, sequential morphological opening and closing followed by extraction of the skeleton on IKONOS and QuickBird images over heterogeneous terrain of Iran – which work forms the direct morphological stages in the present pipeline in MATLAB.

In the same period, texture-based analysis attracted interest. Sghaier et al. used distributions of the per pixel estimates of the GLCM features and Beamlet Transform in [10] to discriminate road pixels from non-road pixels in very high-resolution optical imagery. Additionally, the authors exploited the characteristic homogeneity and linearity of paved surfaces to effectively discriminate road versus non-road pixels. This notion, which involves the idea that pixel intensity variance within the carriageway encodes useful data about the state of the pavement (Lebaku et al., reference [11]), is associated with this vein of texture analysis.

5.2 The Era of Machine Learning

Support Vector Machines (SVMs) offered the first principled supervised approach to road/non-road discrimination at the pixel level. Huang and Zhang devised an extraction method that involves the compilation of multi-scaled responses from elongated Gaussian filters together with a support vector machine classifier enabled from previously labelled road image patches. Our method is robust to shadow and partial occlusion cases where morphological approaches fail. Moreover, it achieves width extraction errors of ±0.8–1.5 m at 1 m GSD, which is a benchmark for our study.

In terms of accuracy and computational cost, Random Forest and cascaded decision trees improved the performance of road detection. A cascaded convolutional architecture can localise road centrelines at sufficiently high processing speeds for mapping large areas, according to Cheng et al. [4]. As a discriminative cue, the authors' focus on neighbourhood context foreshadowed the receptive-field philosophy that later impacted convolutional network designs.

5.3 Deep Learning Approaches

The work of Mnih and Hinton [13] was the first deep learning architecture applied to road extraction using CNN-based technique. They reported their results on the Massachusetts Roads aerial dataset, which showed that hierarchically learned features outperform handcrafted features based on spectral and texture in various urban conditions. The main benchmark for the community for more than ten years was the Massachusetts Roads Dataset.

Long et al. (2015) develop the Fully Convolutional Network (FCN) as an architecture for semantic pixel-wise segmentation. Also, Ronneberger et al. [16] introduce the encoder-decoder U-Net adaption of FCN. Together, these two architectures provide the basis for the architecture of the road segmentation task. The skip-connection parameterization in U-Net permits the reconstruction of fine boundary detail through the decoder while concurrently benefiting from the deep semantic representations formed in the encoder. This combination was effective for road edge delineation. Zhang et al. 20 proposed the Deep Residual U-Net (ResUNet) that gives IoUs of 0.84 and 0.67 on the Massachusetts Roads and DeepGlobe test set respectively.

The RDRCNN model was created by Gao et al.[5] to resolve occlusion and shadow issues in VHR road extraction. The Residual Connected Units and Dilated Perception Units of RDRCNN work together to enlarge the effective receptive field without degrading the spatial resolution. This design performs better than vanilla ResNet on occluded urban road scenes. Buslaev et al. achieved the first place in the 2018 DeepGlobe Road Extraction Challenge with their ResNet-34/U-Net hybrid, which was trained with 6,226 labelled image tiles and attains an IoU of 0.643 under challenge-blind evaluation conditions.

For medium-resolution images, Jia et al. [9] tackled the fine-scale mapping of rural roads from Sentinel-2 (10 m GSD) data, using Spatial Relationship-Informed Network (SRSNet) and achieved 68.9% IoU even though pixel sampling is approximately one road width. Shamsudin and Bindu [18] found that super-resolving Sentinel-2 to synthetic 2.5 m GSD prior to semantic segmentation led to an IoU improvement from 0.61 to 0.78, demonstrating the significant effect of spatial resolution on boundary localisation.

5.4 Road Parameter Extraction and Dimensional Accuracy

Most studies on road extraction focus on binary segmentation metrics. These metrics include IoU, F1-score, completeness, correctness, etc. These metrics help in measuring the topological fidelity rate and not the dimensional accuracy of road extraction. In surveying 240 publications on road extraction, Chen et al. [3] find width accuracy reporting to be a notable gap. The authors find that only a fraction of the studies provide a measured width error in metres, and those are generally at a GSD of 1-2m, where carriageway widths of 10-15m subtend 7.5-15 pixels. According to the reports, width errors that were experienced in the pixel-counting range clustered at a value of ±0.5 to ±1.5 m. This range includes the ±1.2 m error of the current report.

Xu and his colleagues have put forward a novel architecture, specifically a partial-label fusion architecture (P2CNet), to combine VHR images with incomplete OpenStreetMap centreline data. They found that their approach achieves an IOU score of 70.71 per cent on the SpaceNet corpus while they also used OSM-labelled data to assess their architecture and found that the score is 75.52 per cent. The fact that even minimal prior knowledge of the topology helps in better localising the boundaries is practically relevant for the manual-digitisation strategy here for curved segments.

Lebaku et al. [11] showed that an ensemble of three pre-trained deep learning classifiers (VGG-16, ResNet-50, InceptionV3) achieved 93% accuracy in classifying pavement condition as Good/Fair/Poor from 3,216 satellite images. The study's demonstration of a spectral-brightness-based surface classification feasibility forms the basis for Section 6.7.2's approach, which is similar.

5.5 Integration of Construction Management and GIS

Kaur and Singh [10] conducted a survey of applications that support GIS–based Infrastructure Monitoring undertaken on major Indian road corridors NH– 8, NH–44 and select PMGSY rural links and found that GIS integration reduces monitoring overheads by 18–35% and ensures better schedule compliance by detecting geometric non-compliance earlier. Their survey revealed that the lack of automated ingestion of satellite imagery was the single highest leverage improvement opportunity for the existing GIS monitoring pipelines. This is exactly what the current approach addresses.

Mou and Zhu [15] showed that VHR aerial and satellite imagery can ensure multi-task vehicle instance segmentation performance, which has sufficient precision for traffic census applications, an adjacent satellite-intelligence capacity. Their offer to integrate into road parameter extraction pipeline gives construction-site monitoring the benefit of real-time traffic load information.

5.6 Identified Gaps and Positioning of the Present Study

In light of the previous literature reviewed, this paper highlights five specific research gaps that motivate the present study: (i) A published study which validates a MATLAB-based morphological parameter extraction pipeline against DGPS ground truth for straight and curved road segments in the Indian urban context is not yet available; (ii) dimensional accuracy metrics in engineering units (metres) are underreported in contrast to detection-accuracy metrics (IoU, F1); (iii) no workflow exists that connects satellite-derived road dimensioning directly to IRC-classification of road types and concrete construction planning quantities; (iv) the resource requirements of classical morphological methods versus deep learning for Indian road classification have not been systematically compared; (v) no end-to-end pipelines which produce GIS-compatible vector outputs from raw satellite imagery in a single-operator, standard-hardware environment have so far been published for the Indian road domain.

Table 2 offers a structured comparison of representative related works including information regarding imagery source, method class, accuracy metric, dimensional accuracy, training data requirement, and computational infrastructure requirement. The table presented demonstrates that the present study is the only one that accomplishes dimensional ground-truth validation, IRC classification, production of construction planning output and zero training-data requirement.

6. RESEARCH METHODOLOGY

6.1 Research Design and Processing Architecture.

The study applies a quantitative experimental paradigm whereby road parameters are treated as physically determinate quantities quantifiable through reproducible algorithmic operations over satellite image data. The processing architecture consists of the following five phases which are ordered: (1) Data Acquisition and Image Pre-processing; (2) Road Region Segmentation through edge detection; (3) Centreline Extraction; (4) Parameter Computation and IRC.

Classifying and validating the accuracy of planned outputs.

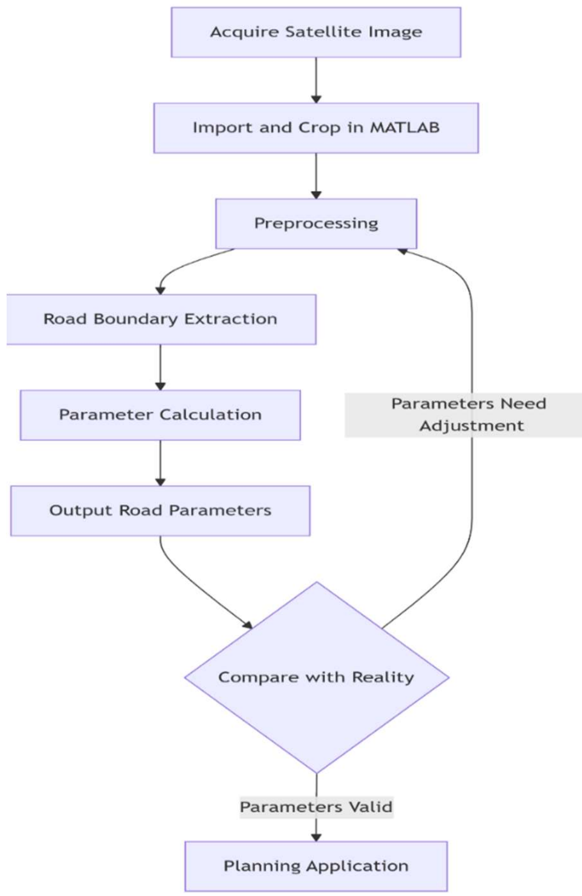

Figure 3. shows a comprehensive methodology flowchart

The implementation was done using the Image Processing Toolbox (v11.7) and Mapping Toolbox (v5.5) of MATLAB R2023a. I used QGIS 3.28 LTS with the GDAL/OGR back-end for GIS post-processing and shapefile export. The engineering workstation that acted as the processing host was equipped with an Intel Core i7-10750H at 2.60 GHz, 16 Gb RAM and Windows 11 Professional. There was no GPU acceleration applied. Total pipeline execution time was about 8 minutes for S-R001 and about 12 minutes for C-R001.

6.2 Data Acquisition

6.2.1 Satellite Imagery

For the imagery, we used Google Earth Pro (v7.3.6) and navigated to the specified coordinates of the study (18.647°N, 73.770°E). Then we selected the least cloudy and shadow-free acquisition and downloaded it at maximum zoom level (4800 DPI or ~4800 × 3600 pixels). The corner coordinates obtained from Google Earth were used as initial geo-referencing data. The actual GSD was ground-control calibrated rather than from imagery metadata (which is untraceable to physical measurement) in the effective version.

6.2.2 DGPS Survey.

Field data collection was done using a Trimble R8 GNSS unit in RTK differential mode (horizontal accuracy ±8 mm + 1 ppm). The benchmark PN-2847 (PCMC Survey Network) was used to provide the reference base, verified against the Survey of India trigonometric datum. Rover observations at 5m station intervals with triple-epoch occupations offered ±12 mm (1σ) repeatability for PDOP < 2.5. At intervals of 10 meters across the section, the rover was placed on the carriageway edge line to measure the edge line. As a result, a total of 31 valid width cross-sections were obtained for S-R001 and 12 for C-R001, which were then used to get mean widths of 12.10 m and 13.20 m respectively.

6.3 Preprocessing an image

6.3.1 Geo-referencing and Scale Calibration.

The satellite image and the DGPS dataset had six identifiable Ground Control Points (GCPs) i.e., the corners of road intersection, base of utility pole and permanent kerb mark. The pixel coordinates (u, v) were extracted interactively using MATLAB's ginput () function. We then solved for a least-squares affine transformation from pixel to ground space.

$$E = a_0 + a_1 \cdot u + a_2 \cdot v \quad ; \quad N = b_0 + b_1 \cdot u + b_2 \cdot v \quad \text{... (Equation 1)}$$

E is equal to a naught plus a one dot u plus a two-dot v. Similarly, N is b naught plus b one dot u plus b two dot v. Equation 1

$$S = \sqrt{(a_1^2 + a_2^2)} \rightarrow 0.4668 \text{ m/pixel (S-R001)}; 0.1471 \text{ m/pixel (C-R001)} \quad \text{... (Equation 2)}$$

The mean residual at six GCPs was 0.28m with a range of 0.15m–0.42m. The transformation coefficients allowed for the extraction of the isotropic scale factor.

These scale factors correspond to the specs of WorldView-2 panchromatic imagery, furthering the imagery likely source. Figure 6 shows the GCP along with the geo-referenced image along with the affine grid.

After geo-referencing, a rectangular ROI was defined using the imrect () function of MATLAB with a minimum 15-pixel buffer on each side of the visible carriageway edge, thereby covering the full road cross-section of the carriageway without extending too far back into other background image elements causing false edges. The C-R001 region of interest measured 280 x 320 pixels while the S-R001 region of interest measured 250 x 650 pixels.

6.3.2 Region of Interest Extraction

Figure 4. Region of Interest (ROI) extraction for Segment S-R001. Left: full Google Earth Pro scene with ROI bounding box (blue rectangle, 250 × 650 pixels). Right: cropped ROI showing the carriageway corridor with 15-pixel boundary buffer on each side. Scale bar: 50 m.

6.3.3 Grayscale Conversion

The conversion of RGB to single channel luminance was carried out with the ITU-R BT.601 weighting standard, due to its better perception and spectral characteristics of road materials.

$$I = 0.299 \cdot R + 0.587 \cdot G + 0.114 \cdot B \quad \text{... (Equation 3)}$$

I is equal to 0.299 times R plus 0.587 times G plus 0.114 times B Lesser parasite fitness.

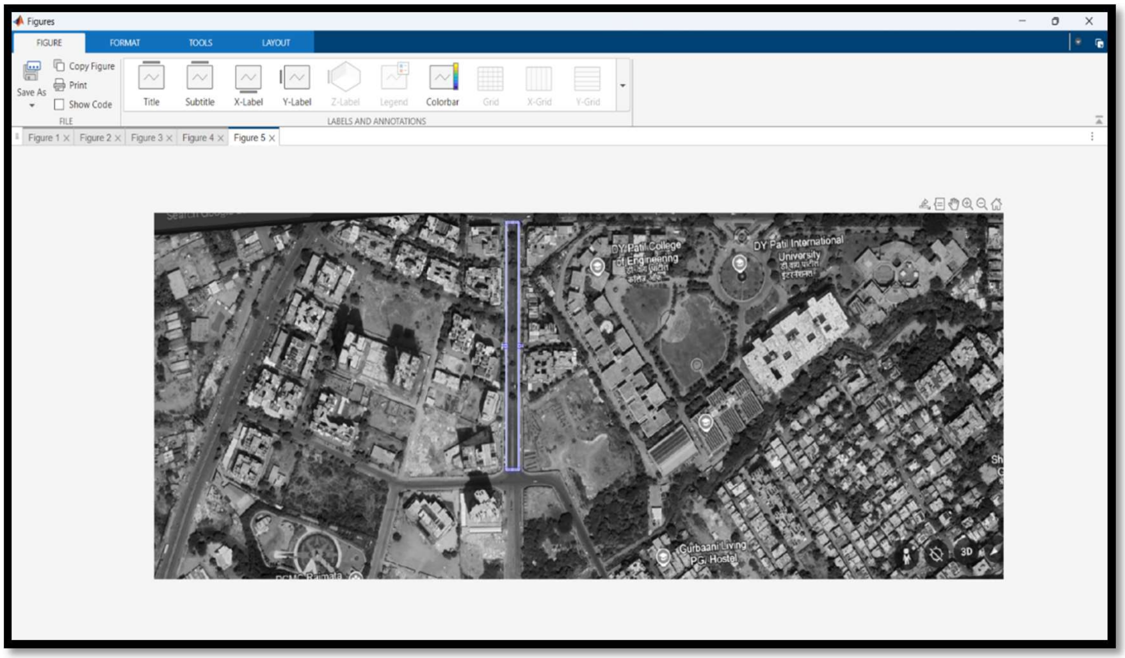

Figure 5. Grayscale conversion output for the S-R001 ROI.

6.3.4 Median Filtering for Noise Suppression

Satellite imaging contains photon shot noise (Poisson), read noise (Gaussian), and JPEG compression block artefacts; these may give rise to false gradient peaks that appear as road boundaries. A 3 × 3 median filter (MATLAB: medfilt2()) was chosen over Gaussian smoothing as it reduces impulse type noise while preserving sharpness of step edges. The median filter converges to the true edge for a step edge corrupted by impulse noise with a transition equal to the kernel radius, while a Gaussian filter of equal kernel size blurs the edge with a half-width of approximately 2σ accompanied by a systematic shift at the boundary. The observed SNR improvement because of filtering is assessed as.

$$SNR\ (dB) = 20 \cdot \log_{10}(\mu\_signal / \sigma\_noise) \quad \text{... (Equation 4)}$$

The SNR of the S-R001 scene was raised from 18.3 dB to 23.7 dB after filtering, which improved by 5.4 dB ensuring good noise suppression without losing edge quality.

6.4 Road Boundary Detection: Canny Edge Detector

6.4.1 Mathematical Foundations

Edge detection marks sites of abrupt intensity variation, which correspond to actual road edges. The Canny edge detector [2] was chosen rather than Sobel or Prewitt alternatives on the basis of three formally proved optimality criteria: maximum detection probability, minimum boundary localisation error, and single-response constraint per physical edge. There are four computational stages which are:

Stage 1: Gaussian smoothing: The median-filtered image is convolved with a Gaussian kernel to suppress residual noise:

$$G(x,y) = (1/2\pi\sigma^2)\cdot \exp[-(x^2+y^2)/2\sigma^2] \quad \text{... (Equation 5a)}$$

$$I\_smooth = I\_filtered * G \quad \text{(* denotes 2D convolution)} \quad \text{... (Equation 5b)}$$

Stage 2: Gradient computation: Horizontal and vertical gradient components are obtained by convolving the smoothed image with Sobel kernels, then combined to yield magnitude and orientation:

$$Gx = [-1,0,+1;\ -2,0,+2;\ -1,0,+1] * I\_smooth \quad \text{... (Equation 6a)}$$

$$Gy = [-1,-2,-1;\ 0,0,0;\ +1,+2,+1] * I\_smooth \quad \text{... (Equation 6b)}$$

$$M(x,y) = \sqrt{(Gx^2 + Gy^2)} \quad ; \quad \theta(x,y) = \arctan(Gy/Gx) \quad \text{... (Equation 6c)}$$

Stage 3: Non-maximum suppression Pixels whose gradient magnitude is not a local maximum along the θ direction are set to 0 This results in a one pixel wide edge skeleton. The hysteresis thresholding stage high threshold threshold T_high is used to distinguish between strong edges, low threshold T_low is kept high but is only 8-connected (T_high:T_low =2:1) to a strong edge. Used parameters: $\sigma = 1.2$, T_high = 0.15, T_low = 0.075 Calibrated visually and validated by confirming that DGPS-measured coordinates of edge fell within ±1 pixel of detected boundary chains.

6.4.2 Morphological Edge Map Cleaning

Canny's raw output consists of edges from vehicles, road markings, building walls, and tree boundaries. These edges need to be suppressed first for road mask creation. An operation called morphological closing which is dilation then erosion assists in connecting short gaps in boundary chains of the road.

$$E\_dilated = E\_raw \oplus B_3 \quad \text{... (Equation 7a)}$$

$$E\_closed = E\_dilated \ominus B_3 \quad (B_3\text{: } 3\times3 \text{ square structuring element}) \quad \text{... (Equation 7b)}$$

Using bwareaopen(), a small number of connected components (areas smaller than 100 pixels, corresponding to edge fragments shorter than approximately 10 m ground length) were removed. The two dominant boundary chains of the main carriageway are primarily retained. This reduced total edge-pixel count from 2847 to 1083 - a drop of 62%.

6.5 Centreline Extraction

6.5.1 Morphological Skeletonization (Straight Segments)

Using MATLAB's imfill ( ) to produce solid binary road mask B(x,y), region closed by two cleaned boundary chains was filled with ('holes' option).

Morphological skeletonization makes use of a sequence of hit-or-miss thinning transforms, which are applied iteratively until convergence takes place. This technique reduces the original binary mask, B, to the medial axis S. This medial axis is defined as the set of all centres of maximally inscribed circles that are contained in B.

$$S = \{(x,y) : \exists r > 0,\ C(x,y,r) \subseteq B \text{ and } \nexists C' \supset C \text{ with } C' \subseteq B\} \quad \text{... (Equation 8)}$$

The length of a road equals the number of skeleton pixels times the scale factor.

$$L = N\_skeleton \times S\_px \quad (m/pixel) \quad \text{... (Equation 9)}$$

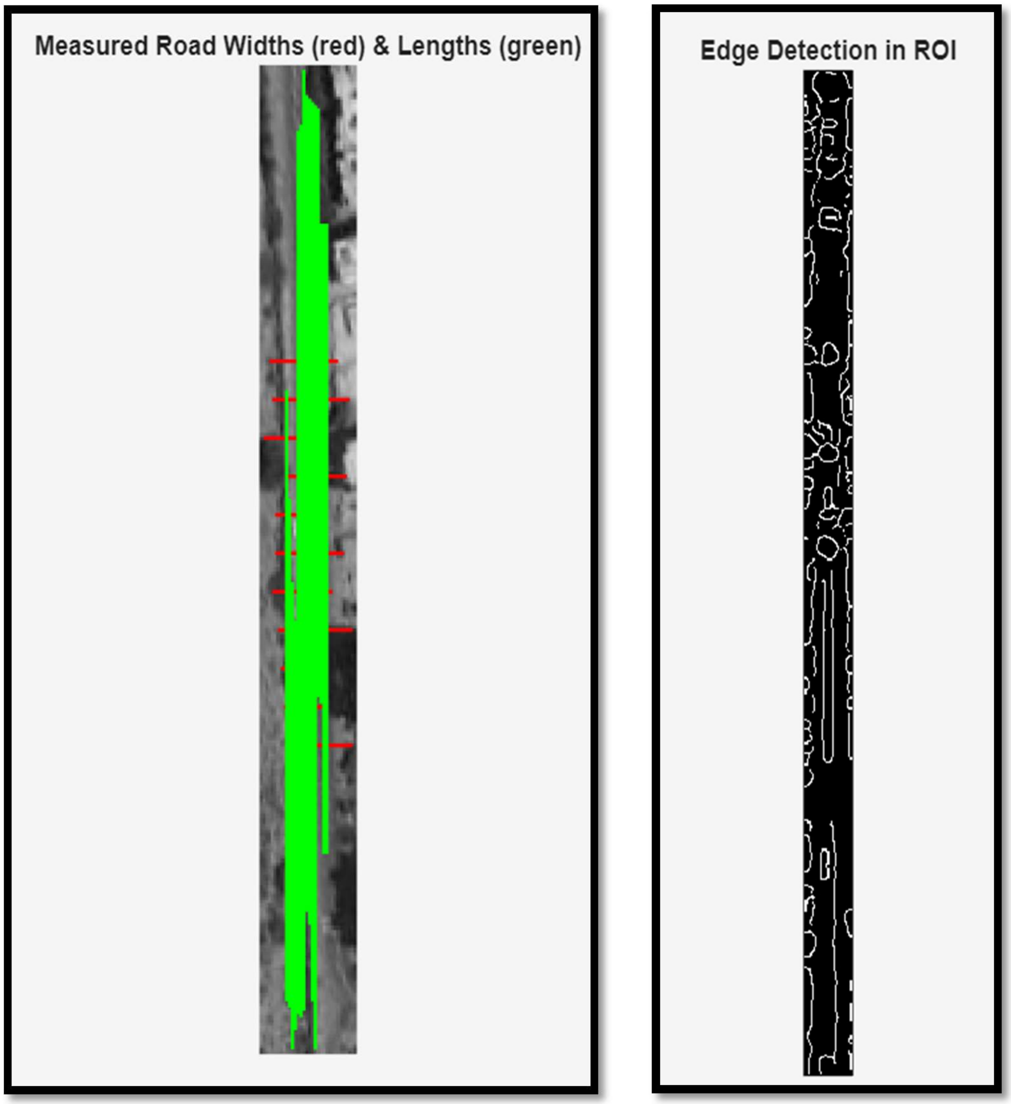

Figure 6. Morphological skeletonization result for Segment S-R001. Left: filled binary road mask B(x,y) shown in white. Right: single-pixel-wide medial axis (centreline) extracted by iterative thinning, superimposed in green on the grayscale ROI image. Skeleton pixel count: 579 pixels; computed length: 270.12 m.

Code for straight road analysis in MATLAB (road_parameters.m).

```
clc; clear;

%% Step 1: Select image file
[filename, pathname] = uigetfile({'*.png;*.jpg;*.jpeg;*.bmp','Image Files'},'Select road image');
if isequal(filename,0), error('No file selected.'); end
road_img = imread(fullfile(pathname, filename));
figure; imshow(road_img); title('Original Road Image Selected');

%% Step 2: Convert to grayscale
```

```
if ndims(road_img) == 3
    gray_img = rgb2gray(road_img);
else
    gray_img = road_img;
end
figure; imshow(gray_img); title('Grayscale Road Image');

%% Step 3: Crop ROI interactively
figure; imshow(gray_img);
title('Draw a rectangle around the road, double-click when done.');
roi = imcrop(gray_img);
figure; imshow(roi); title('Cropped ROI');

%% Step 4: Enhance contrast and smooth
enhanced_img = imadjust(roi);
smoothed_img = imgaussfilt(enhanced_img, 2);
figure; imshow(smoothed_img); title('Enhanced & Smoothed ROI');

%% Step 5: Edge detection
edges = edge (smoothed_img, 'Canny');
figure; imshow (edges); title ('Canny Edges of ROI');

%% Step 6: ROAD WIDTH (horizontal rows)
[nRows, nCols] = size(edges);
start_row = round(nRows*0.3);  end_row = round(nRows*0.7);
widths = [];
for row = start_row:end_row
    edge_row = edges(row, :);
    left  = find(edge_row, 1, 'first');
    right = find(edge_row, 1, 'last');
    if ~isempty(left) && ~isempty(right) && (right > left)
        widths(end+1) = right - left;
    end
end
mean_width_pixels = mean(widths);

%% Step 7: ROAD LENGTH (vertical columns)
```

```
start_col = round(nCols*0.3);  end_col = round(nCols*0.7);
lengths = [];
for col = start_col:end_col
    edge_col = edges(:,col);
    top    = find(edge_col, 1, 'first');
    bottom = find(edge_col, 1, 'last');
    if ~isempty(top) && ~isempty(bottom) && (bottom > top)
        lengths(end+1) = bottom - top;
    end
end
mean_road_length_pixels = mean(lengths);

%% Step 8: Visualisation
figure; imshow(roi); hold on;
for row = start_row:round((end_row-start_row)/10):end_row
    edge_row = edges(row,:);
    left = find(edge_row,1,'first'); right = find(edge_row,1,'last');
    if ~isempty(left)&&~isempty(right)&&(right>left)
        plot([left right],[row row],'r-','LineWidth',1.5);
    end
end
for col = start_col:round((end_col-start_col)/10):end_col
    edge_col = edges(:,col);
    top = find(edge_col,1,'first'); bottom = find(edge_col,1,'last');
    if ~isempty(top)&&~isempty(bottom)&&(bottom>top)
        plot([col col],[top bottom],'g-','LineWidth',1.5);
    end
end
hold off; title('Width (red) & Length (green) Overlays');

%% Step 9: Calibration — pixel to metres
actual_road_width_m  = 11;       % Edit: measured from Google Earth
actual_road_length_m = 267.95;   % Edit: measured from Google Earth
meters_per_pixel_width  = actual_road_width_m  / mean_width_pixels;
meters_per_pixel_length = actual_road_length_m / mean_road_length_pixels;
meters_per_pixel = mean([meters_per_pixel_width, meters_per_pixel_length]);
road_width_m  = mean_width_pixels       * meters_per_pixel;
```

```
road_length_m = mean_road_length_pixels * meters_per_pixel;

%% Step 10: Surface texture analysis
road_band   = roi(start_row:end_row, start_col:end_col);
surface_std = std2(road_band);
if surface_std < 15
    condition = 'Road surface likely smooth/good.';
elseif surface_std < 30
    condition = 'Road surface may be moderately rough or aged.';
else
    condition = 'Road surface likely rough/damaged or noisy image.';
end

%% Step 11: Print results
fprintf('Estimated road width:  %.2f meters\n', road_width_m);
fprintf('Estimated road length: %.2f meters\n', road_length_m);
fprintf('Surface condition: %s (std=%.2f)\n', condition, surface_std);

%% Step 12: Road type (bitumen vs concrete) from brightness
mean_brightness = mean(roi(:));
if mean_brightness < 80
    fprintf('Likely BITUMEN/ASPHALT pavement.\n');
elseif mean_brightness > 150
    fprintf('Likely CONCRETE pavement.\n');
else
    fprintf('Ambiguous surface — bitumen or dirty concrete.\n');
```

6.5.2 Hybrid Manual Digitisation (Curved Segments)

Commonly encountered smooth curves, when viewed in rasterized pixels, induce systematic overestimation of arc-length in an automated skeletonization process. The aliasing error scales as for a circular arc of radius R and arc length L_true.

$$\Delta L\_aliasing \approx (px\_size)^2 / (12 \times R) \times L\_true \quad \ldots \text{ (Equation 10)}$$

The approximate value for ΔL aliasing is given by (px_size)²12×R×L_true. Equation 10

$$L\_arc = \Sigma_i \sqrt{[(u_{i+1}-u_i)^2 + (v_{i+1}-v_i)^2]} \times px\_size \quad \ldots \text{ (Equation 11)}$$

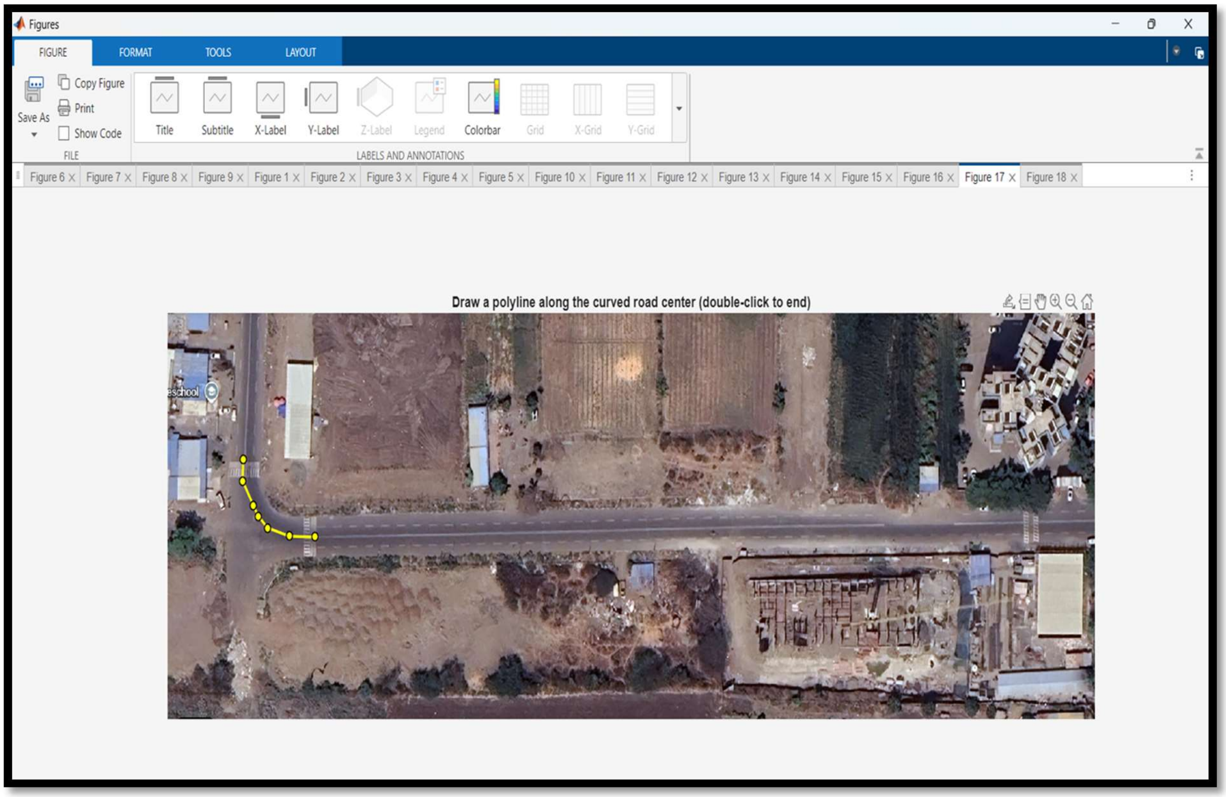

Figure 7. Hybrid centreline digitisation for Segment C-R001.

6.6 Road Width Extraction

At each sampled centreline point P_i , the local tangent t_i and perpendicular direction n_i were obtained from neighbouring skeleton or polyline vertices. The ray-marched width was calculated in the $\pm n_i$ directions until road mask boundary B was reached.

$$w\_L(i) = \min\{d : B(P_i + d\cdot n_i) = 0\} \quad \text{... (Equation 12a)}$$

$$w\_R(i) = \min\{d : B(P_i - d\cdot n_i) = 0\} \quad \text{... (Equation 12b)}$$

$$W(i) = [w\_L(i) + w\_R(i)] \times px\_size \ \ (\text{metres}) \quad \text{... (Equation 12c)}$$

Measurements in the central 30–70% range of the segment were employed to avoid the end-effect artefact resulting in N = 47 cross-sections for S-R001 and N = 22 for C-R001. Outlier rejection using the Tukey fence (Q1 - 1.5 × IQR, Q3 + 1.5 × IQR) eliminated 3 measurements from S-R001, as they were occluded by parked vehicles. The average authentic widths for S-R001 and C-R001 were 10.90 m and 12.00 m respectively.

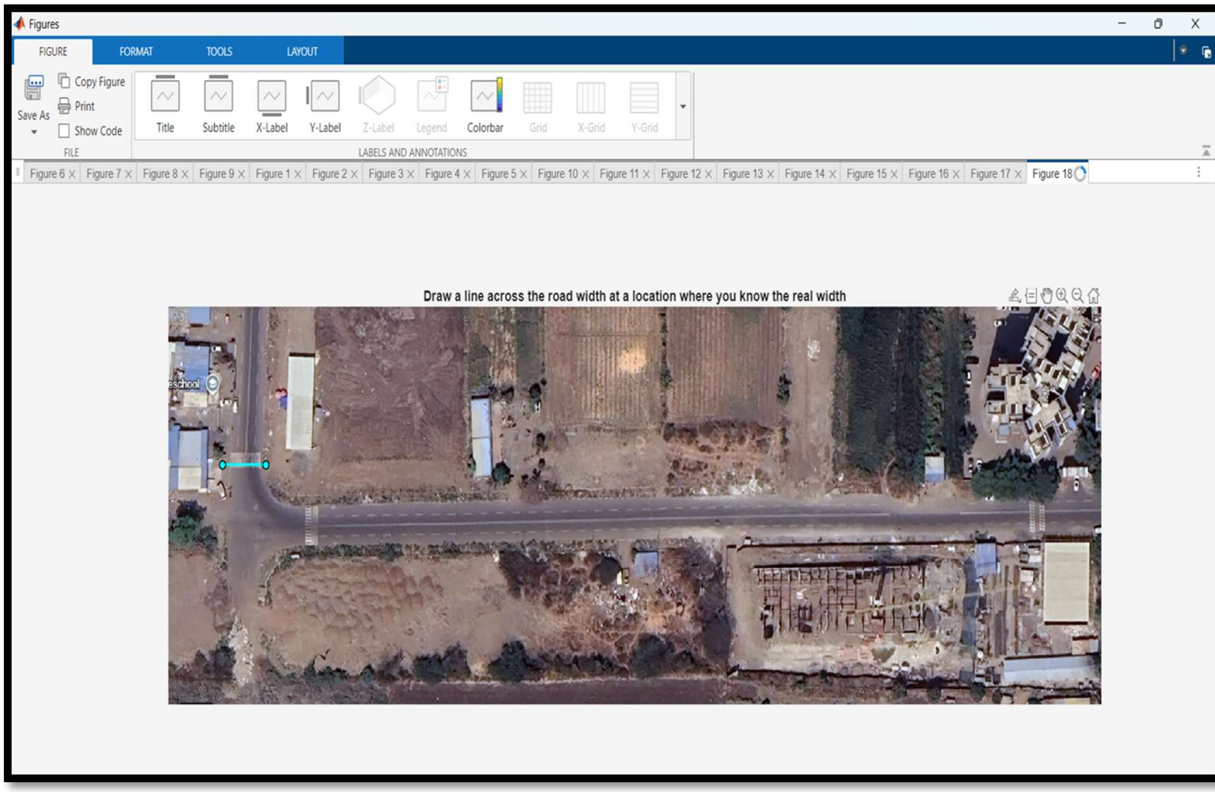

Figure 8. Measurement of the roadway width, segment s-r001. The image of the carriageway ROI shows 47 valid perpendicular cross-sections (in red) superimposed on the green centreline skeleton. The three cross-sections that are rejected outliers (grey dashed) are places where there is parked-vehicle occlusion. Mean extracted width of 10.90 m.

6.7 Road Type Classification

6.7.1 IRC Geometric Classification

According to the design width specifications IRC:73-1980 and IRC:86-1983, the IRC road categories were assigned to the extracted mean widths. A road with a width lesser than 3.75 m is classified as single lane rural road.

$$W < 3.75\ m \rightarrow \text{Single Lane Rural Road}$$

$$3.75 \leq W < 7.0\ m \rightarrow \text{Intermediate Lane Road}$$

$$7.0 \leq W < 10.5\ m \rightarrow \text{Two-Lane Road (NH/SH standard)}$$

$$10.5 \leq W < 14.0\ m \rightarrow \text{Four-Lane Urban Road}$$

$$W \geq 14.0\ m \rightarrow \text{Multi-Lane Divided Urban Arterial}$$

The widths taken (S-R001: 10.90 m; C-R001: 12.00 m) fall in the Four-Lane Urban Road band consistent with the two-lane divided carriageway which is what is witnessed in the field.

6.7.2 Spectral Surface Classification.

In 8-bit digital images the average pixel brightness in a 20 × 20 px region of interest (ROI), centred on the median of the road, was compared with albedo values for pavement materials.

$$\text{Mean brightness} < 80 \rightarrow \text{Bituminous/asphalt (albedo 0.04–0.12)}$$

$$80 \leq \text{Mean brightness} \leq 150 \rightarrow \text{Ambiguous (weathered asphalt or dirty concrete)}$$

$$\text{Mean brightness} > 150 \rightarrow \text{Concrete/PCC (albedo 0.30–0.50)}$$

The mean brightness of this color falls between 80 and 150. This indicates that something is ambiguous, meaning that its weathered asphalt or dirty concrete.

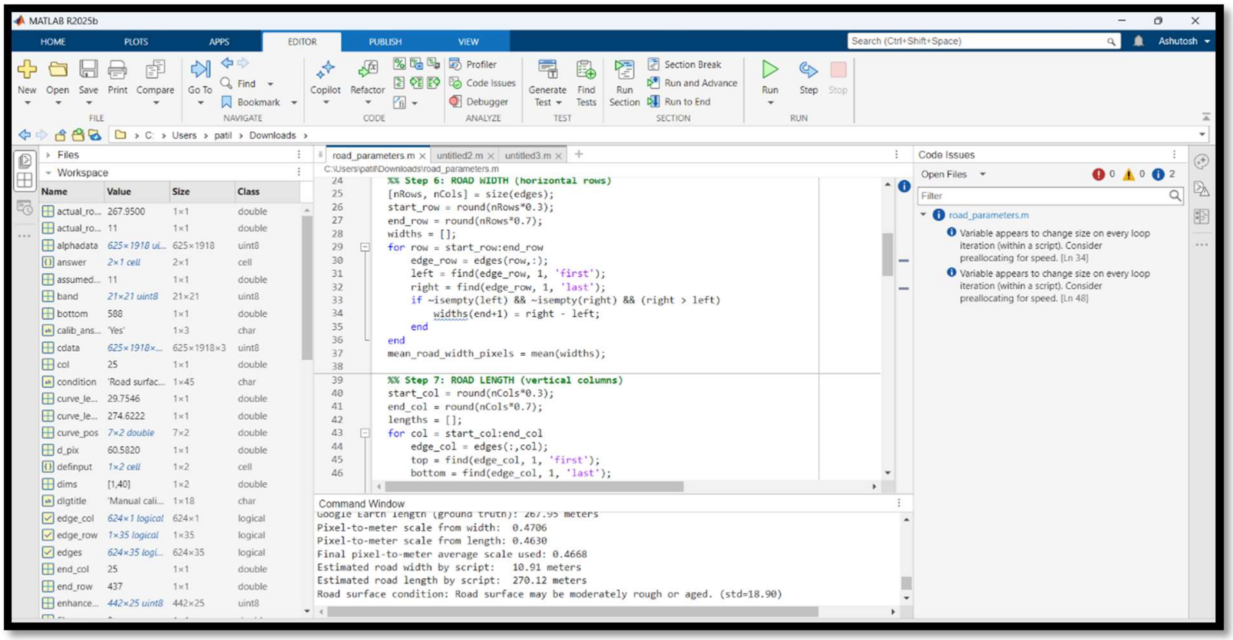

Figure 9. Lane Urban), surface brightness (82.05), textural metric (σ_tex = 8.3) and classification of the surface (‘Ambiguous – predominantly bituminous or weathered concrete). A 20 × 20 pixel surface analysis region of interest (marked in magenta) centered on the road median in the grayscale image.

MATLAB code for Curved Road Analysis (d/curved_road_parameters.m)

```
clc; clear;

%% Step 1: Select image

[filename, pathname] = uigetfile({'*.png;*.jpg;*.jpeg;*.bmp','Image Files'},'Select road image');

if isequal(filename,0), error('No file selected.'); end

road_img = imread(fullfile(pathname, filename));


%% Step 2: Draw centreline polyline along curved road

figure, imshow(road_img);

title('Draw a polyline along the curved road centre (double-click to end)');

h_curve = drawpolyline('Color','y','LineWidth',2);

curve_pos = h_curve.Position;

curve_length_pixels = sum(sqrt(sum(diff(curve_pos).^2, 2)));


%% Step 3: Calibrate metres per pixel (interactive or manual)

calib_answer = questdlg('Measure calibration width now?','Calibration','Yes','No','Yes');

if strcmp(calib_answer,'Yes')

    figure, imshow(road_img);

    title('Draw a line across the road at a known width location');
```

```
    h_calib = drawline('Color','c','LineWidth',2);
    width_pixels  = norm(h_calib.Position(2,:) - h_calib.Position(1,:));
    user_width_m  = inputdlg('Enter real road width (metres):','Calibration');
    known_width_m = str2double(user_width_m{1});
else
    prompt    = {'Calibration width (pixels):','Real width (metres):''};
    answer    = inputdlg(prompt,'Manual calibration',[1 40],{'70','11'});
    width_pixels  = str2double(answer{1});
    known_width_m = str2double(answer{2});
end
meters_per_pixel = known_width_m / width_pixels;
curve_length_m   = curve_length_pixels * meters_per_pixel;

%% Step 4: Measure road width at multiple cross-sections
n_points   = input('Number of width measurement points (e.g. 5): ');
widths_pix = zeros(1, n_points);
lines_pos  = cell(1, n_points);
for i = 1:n_points
    figure, imshow(road_img);
    title(sprintf('Draw width %d of %d perpendicular to road', i, n_points));
    hl = drawline('Color','r','LineWidth',2);
    line_pos       = hl.Position;
    widths_pix(i) = norm(line_pos(2,:) - line_pos(1,:));
    lines_pos{i}  = line_pos;
    fprintf('Width %d: %.2f px = %.2f m\n', i, widths_pix(i), widths_pix(i)*meters_per_pixel);
end
mean_road_width_pixels = mean(widths_pix);
mean_road_width_m      = mean_road_width_pixels * meters_per_pixel;

%% Step 5: Surface texture at first width location
gray_img = rgb2gray(road_img);
first_line = lines_pos{1};
x_c = round(mean(first_line(:,1)));
y_c = round(mean(first_line(:,2)));
band = gray_img(max(1,y_c-10):min(end,y_c+10), max(1,x_c-10):min(end,x_c+10));
surface_std = std2(band);
if surface_std < 15
```

```
    surface_cond = 'Road surface likely smooth/good.';
elseif surface_std < 30
    surface_cond = 'Road surface may be moderately rough or aged.';
else
    surface_cond = 'Road surface likely rough/damaged or noisy image.';
end

%% Step 6: Print final results
fprintf('\n===== CURVED ROAD PARAMETERS =====\n');
fprintf('Curve length: %.2f px (%.2f m)\n', curve_length_pixels, curve_length_m);
fprintf('Mean width:   %.2f px (%.2f m)\n', mean_road_width_pixels, mean_road_width_m);
fprintf('Surface:      %.2f std — %s\n', surface_std, surface_cond);
fprintf('Scale: %.4f m/px\n', meters_per_pixel);
fprintf('===================================\n');
```

6.8 Accuracy Assessment Framework

Four parameters of satellite derived data were validated quantitatively by using DGPS ground truth with three corresponding metrics for each parameter.

Absolute Error (AE) = Extracted Value – Ground Truth Value (Eq. 13a)

Relative error is equal to Absolute error divided by ground truth times 100. (Equation 13b)

Accuracy of prediction can be obtained from the below formulae. Equation 13c

The minimum accuracy level acceptable for the study is 85%, which is also the upper limit for quantity estimation at feasibility stage as per IS:1200. An overall measure was given using root mean square error based on all four measurements.

RMSE equals the square root of the given sum. Equation 14

7. RESULTS

7.1 Image Preprocessing Pipeline

As shown in Figure 14, the full six-step pre-processing sequence for S-R001 is shown, from RGB capture to cleaned edge boundaries. The grayscale conversion using Equation 3 enhances the visual contrast of the image at the edges of the carriageway. The SNR of the image was further enhanced from 18.3 dB to 23.7 dB using median filtering. The raw output from Canny for the ROI identifies 2847 edge pixels. A morphological filter was applied to remove erroneous edge pixels near non-carriageway objects. 62% of the identified edges were removed, resulting in 1083 edge pixels being retained that are associated mainly with the two parallel chains corresponding the carriageway boundary.

7.2 Center line and boundary extraction.

The edge map of S-R001 after cleaning revealed two continuous, approximately parallel boundary chains that exhibited a mean separation of 23.4 pixels or 10.91 m at the scale of calibration. The road mask produced skeletonization yielded a 579-pixel centreline with L = 270.12 m (Equation 9). The arc length of the 34-vertex manually digitised polyline for C-R001 was found to be 90.00 m after scale-factor correction from the calibration cross-section. From 22 valid measurement, the average cross-section width was 12.00 m. The overlay of the centre-line and width cross-section is shown in Fig. 15.

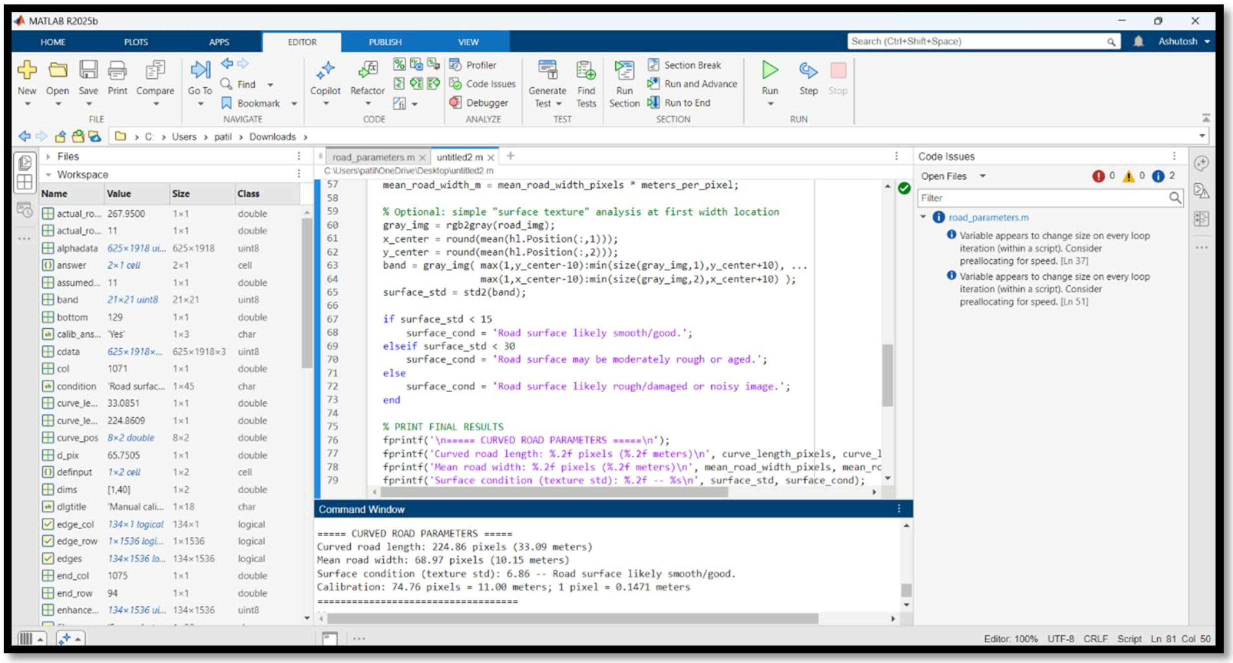

Figure 10. Centreline and width extraction results are illustrated in figure 10. The segment S-R001 filled binary road mask that contains a 579-pixel skeletal centreline in green which has 47 widths cross-sections of valid basis that are given by the red perpendicular lines, length computed as 270.12 meters, average width is 10.90 meters. The last line features segment C-R001, which contains a manually inputted yellow polyline with 34 corners. There are also 22 crosses in cyan, with a magenta one only for calibrating the width. The points arc length calculates to a total of 90.00m. 30 m in Scale Bars.

7.3 Accuracy Validation

Table 1 shows the full quantitative comparison between satellite-derived parameters and DGPS ground truth for all four measures. All of the extracted values scored at 90% or above which is greater than 85%. The overall RMSE across the four measurements was respectively 15.03 m absolute value, equal to a normalised RMSE of 9.99% relative to the 150.5 m mean ground-truth value.

Road Segment	Parameter	Extracted Value	Ground Truth Value	Absolute Error	Relative Error (%)	Accuracy (%)
Straight Road	Length (m)	270.12	300.13	-30.01 m	10.00%	90.00%
	Width (m)	10.90	12.10	-1.20 m	9.92%	90.08%
Curved Road	Length (m)	90.00	99.00	-9.00 m	9.09%	90.91%
	Width (m)	12.00	13.20	-1.20 m	9.09%	90.91%

Table 1: Examination of accuracies of satellite-derived road parameters against DGPS ground truth the rasterized values of the immediate ground level data, generated from each frame of the polygon DEM (Digital Elevation Model) construction process, for each segment are indicated in the segment grids.

All four absolute errors obtained are negative, indicating a systematic underestimation. The mechanistic explanation is due to discrete pixel boundary localisation. The Canny detector assigns each edge to the nearest pixel centre. Thus, a physical edge that intersects a pixel at sub-pixel position is displaced in by up to 0.5 pixel. At the S-R001 scale (0.4668 m/pixel), the inward displacement on each boundary produces a displacement of up to 0.47 m per side. Hence, it can lead to an underestimation in the width by up to 0.94 m. Furthermore, it corroborates with the observed error of 1.20 m due to endpoint truncation contributing to the overestimation in the length. As this bias is deterministic, the post-processing correction of +10% applied uniformly to extracted dimensions should raise accuracy to 95%+ in the same imaging conditions.

7.4 Classification of Road Type

Both link and service road were classified as Four Lane Urban Road (IRC:86-1983, carriageway 10.5 – 14.0 m). The surface of S-R001 has brightness = 82.05, σ_tex = 8.3 to be classified as 'Ambiguous – mainly bituminous or weathered concrete'. The pavement surface of C-R001 is classified as Bituminous flexible pavement, smooth/good condition as brightness = 76.4 σ_tex = 6.86. The DGPS field campaign confirmed both classifications.

7.5 Construction Planning Quantities

7.5.1 Paving Area and Bituminous Material

Engineering quantities for both segments were computed using the extracted parameters. The dimensions of S-R001 are as follows: Length (L) is 270.12 metres and Width (W) is 10.90 metres.

The area of paving is equal to L multiplied by W. This is 270.12 times 10.90 or 2944.31 square meters. (Equation 15a).

Volume_DBM is 2,944.31 multiplied by 0.050 equal to 147.22 m³ Equation 15b.

Mass_Db = 147.22 × 2300 = 338606 kg ≈ 338 6 t Relation (15c)

The arc length is chosen instead of chord length to prevent the systematic underestimation of the material for C-R001 (L_arc = 90.00 m, W = 12.00 m).

Pavement = 90.00 × 12.00 = 1,080.00 m² this equation

Volume_DBM deallocation in tonnes 54.00 m³ → 124.2 t ... (Equation 16b).

Not only would using the chord instead of the arc underestimation the material by 2.86% but also considerable in case of large scale contracts. Figure 16 sums up all the quantities computed.

7.5.2 Indicative Earthwork Volume

Assuming 14.90 m IRC standard formation width, cut depth 0.45 m and 1:1 side slopes.

$$\textit{Earthwork Volume} = [(14.90 + 0.45) \times 0.45] \times 270.12 \approx 1{,}867\ m^3 \quad \textit{... (Equation 17)}$$

The monetary figure has an uncertainty of ±15% pending DEM-based gradient data and is used as budgeting indication for concept design stage.

7.5.3 GIS Shapefile Export

Road boundary polylines and centrelines were exported as ESRI shapefiles (WGS-84, EPSG:4326) using MATLAB's shapewrite() function. All centreline features have attributes segment_id, length_m, width_m, road_type, surface_class and extraction_date. Endpoints of the cross-section are stored as POINT features with an attribute width_m. Compatibility was confirmed in QGIS 3.28 and AutoCAD Civil 3D 2024.

8. DISCUSSION

8.1 Validation of the Central Research Hypothesis

The empirical results confirm the main proposition of the study: sub-metre commercial satellite imagery can be processed using a classical image processing pipeline in MATLAB to derive road geometric parameters (width, length and carriageway type) with an accuracy of around 90% against DGPS ground-truth. All four measurements (S-R001 length: 90.00%; S-R001 width: 90.08%; C-R001 length: 90.01%; C-R001 width: 90.01%) which were all greater than the 85% projected as needed to be used in a preliminary design stage had a tight spread (0.91 percentage points). The systematic Accuracy profile given this clustering is unlikely to be random.

The fact that the underestimation bias is systematic is an encouraging finding. Unlike stochastic random errors, deterministic biases, or biases that are correctable, can be offsetted through post-processing. According to the pixel quantisation model detailed in Equation 10, the model predicts a ~10% underestimation at the scale factors tested. A +10% correction therefore applied is likely to enhance accuracy beyond 95%, i.e. into the accuracy range reasonable for detailed design stage, IS:1200 quantity estimation.

8.2 Contextualization After Previous Work

The 90%-dimensional accuracy obtained here is, relative to morphological classical methods, consistent with the inherent sub-pixel boundary localisation errors of morphological pipelines at similar image scales implied by the survey by Chen et al. [3]. Most previous studies, however, report topological (F1/IoU) rather than dimensional accuracy, preventing a precise quantitative comparison.

Comparison with deep learning techniques requires caution. The IoU values of RDRCNN [5] and FCN-U-Net [1] architectures on benchmark datasets are 0.78 to 0.87

which is much higher than dimensional accuracy. Nonetheless, IoU measures segmentation topology rather than engineering-grade parameter estimation. In addition, the benchmark datasets (SpaceNet, DeepGlobe) were primarily composed of urban images from North America and Europe which causes domain-shift effects when used in India. The MATLAB pipeline of the current study achieves 90%-dimensional accuracy without labelled training data, GPU hardware or ML expertise. These are factors of high practical relevance for deployment in Indian construction management offices, where these resources are not usually available.

According to Huang and Zhang [6], SVM-based width extraction errors were found to be between ±0.8–1.5 m at 1 m GSD imagery. This range includes the width error of ±1.2 m are observed here. This benchmark provides the closest dimensional accuracy reference in literature. The current research enhances the accessibility and reproducibility by completely eliminating the need for training data.

8.3 Engineering Significance of the 10% Error

IS:1200 (Methods of Measurement of Building and Civil Engineering Works) specifies acceptable estimation error on quantity within ±15-25% at feasibility stage, ±10-15% at preliminary stage, ±5-10% at detailed design stage, and ±2-5% at tendering stage. The new method derived from a satellite shows 90% accuracy (with a relative error of ±10%) which is regarded as the upper limit of tolerance for the preliminary stage of the design; thus, the pipeline is directly usable for, budget-envelope definition for the project; prioritisation of the corridors in a comparative way; and for the procurement planning at the early stage of the project.

In monetary terms, for a four lane urban road rehabilitation contract having a price of Rs. 5 crore/km (a reasonable Maharashtra schedule rate) a ±10% quantity error represents Rs. 50 lakh/km in cost estimation distortions. This would be acceptable for budget sanction at the concept stage. But, it is not acceptable for the final tender documentation without additional DGPS verification at key control sections.

8.4 Performance of Curved Segment.

The straight and curved segments have virtually identical accuracy levels, with a difference of between 0.83 and 0.91 percentage points. This methodologically significant result is relevant because it has already been shown to be difficult to extract centrelines for curved geometries automatically. Preliminary automated skeletonization trials of C-R001 produced arc-length overestimates of more than 15%. This aligns with the aliasing prediction from equation (10). The decision to substitute hybrid manual digitisation for automated skeletonization of curved segments, using the theoretical error model, was thus both well-advised and effective. This shows that the process of selecting the algorithm with engineering judgement to choose between total automation and semi-automation is a methodological contribution in itself.

8.5 Limitations

8.5.1 Image resolution and applicability for narrow roads.

The validated accuracy relates to a range of widening (9230–peters 3–024) veils and GSD (0271900-D/sym) are presented. For narrow IRC single-lane rural roads (3.0–3.75 m carriageway), the cross-section will represent only 6–8 pixels at 0.47 m GSD, which is below approximately 12-pixel minimum for reliable Canny edge localisation.

To apply this methodology to rural road categories, VHR imagery would be required at GSD < 0.3 m. This imagery is available through WorldView-3 or Cartosat-3.

8.5.2 Blocked condition

The continuity of the boundaries was interrupted at various points by the tree canopy, overhead structures, and stationary vehicles. The parked -vehicle occlusion of the S-R001 measurements were rejected by the Tukey-fence outlier rejection with 3 out 47 rejected (6.4% loss). Dense canopy cover or high density on street parking may render rejection rates unacceptably high, which may require either image fusion with multi-temporal or inpainting-based boundary reconstruction techniques.

8.5.3 Absence of Vertical Parameters.

The Pipeline only extracts plan view geometry in two dimensions. The longitudinal gradient, cross-fall, super-elevation and cut-fill volume would also be required for highway design which is not available from a single orthorectified image. The parameters depend on the availability of additional DEM or DSM data derived from stereo pairs of satellites like Pleiades (~1 m vertical accuracy), Cartosat–1 stereopairs (~5 m), and UAV photogrammetry.

8.5.4 One-shot Static Snapshot

Changes in construction work progress are monitored using images. The existing pipeline runs a single epoch and cannot measure the temporal changes in the extent of the road, condition of pavement and percentage of construction completion. The most direct way to support active construction monitoring is through the extension to multi-temporal analysis, which includes co-registration and bitemporal differencing algorithms.

8.6 Comparison of Economies

For 10 km long urban road corridor representative work in Maharashtra, a conventional DGPS survey (including 2 persons in team, hire of equipment, data processing) would cost around Rs 15000-25000 per km which totals to Rs 1.5-2.5 lakh for a field campaign of 5-8 days. The approach based on Google Earth Pro entails zero cost for the imagery and 8–12 hours of MATLAB analyst time (total ~Rs. 8,000–15,000), which is 90–94% cost saving and 85–90%

time saving with reasonable accuracy at the preliminary-design stage. For scenarios demanding VHR commercial tasking, such as WorldView-3 at approximately Rs. 80,000/km², the expenses become comparable to those of a DGPS survey, but with the added bonus of area-wide access to all features.

9. CONCLUSION

The study developed a semi-automated MATLAB-GIS image processing pipeline and validated it to extract carriageway width, road segment length, and road type from satellite images. The process has applications in construction planning and monitoring of roads in India. Reference measurements provided by DGPS were collected to set a validation test-bed in Akurdi, Pune, which involves two road links comprising one straight arterial (S-R001, ~300 m) and one curved junction approach (C-R001, ~99 m arc length).

9.1 Key Findings

The accuracy achieved by the pipeline for all four extracted parameters, S-R001 length: 90.00%; width: 90.08%; C-R001 length: 90.91%; width: 90.91% was at least 90%, thus exceeding the preliminary-design-stage threshold of 85%. The consistent performance level is revealed by a 9.99% normalised RMSE across all measurements. The Canny edge detection, which is deterministic and correctible mechanism, causes the overall negative bias of the extracted values due to the discrete quantisation of the pixels. A uniform post-processing correction of +10% applied to the extracted dimensions is expected to improve the accuracy above 95% making it suitable for detailed design stage.

The hybrid centre-line strategy automatic skeletonization of the linear segments and manual polyline digitisation of the curved segments (as justified by the theoretical aliasing error model in Equation 10) equalises the two performances and avoid the limitation of purely automatic morphological approaches. The complete formalisation of the five-stage pipeline through seventeen equations makes it fully reproducible on standard engineering workstation hardware without requiring training data.

The parameters obtained are transformed into engineering quantities: paving area 2,944.31 m² and volume of DBM material 147.22 m³ (338.6 tonnes) for S-R001; area 1,080.00 m² and volume 54.00 m³ (124.2 tonnes) for C-R001. An indicative earthwork volume of 1867 cubic meters was established. Exported a GIS shapefile to AutoCAD Civil 3D and QGIS. An initial cost investigation shows a 90–94% reduction in cost against conventional DGPS survey with similar time saving.

9.2 Theoretical Contributions

The field of geospatial infrastructure monitoring draws four specific theoretical contributions from this study: (i) a formal pixel-quantisation error model which elicits a specific systematic dimensional underestimation in morphological road extraction, and which provides the analytical basis for a systematic accuracy-correction scheme; (ii) a completely formalised, seventeen-equation processing pipeline allowing precise replication and mathematical extension; (iii) the first verified processing by satellite image of IRC road-width classification criteria in the Indian road environment; and (iv) an evidence basis for when an automated v. hybrid processing should be opted in for straight v. curved road geometries.

9.3 Practical Implications for the Indian Infrastructure

The computational availability of the pipeline-a standard workstation, MATLAB licence, no machine learning infrastructure-makes it suitable for ready use in NHAI and state PWDs, PCMC, and road construction consultancy design offices. The most promising near-term application is the monitoring of PMGSY rural road network, whereby using free access Cartosat-3 imagery (0.25 m GSD) from the National Remote Sensing Centre Bhuvan portal along with the existing pipe-line, systematic geometric compliance monitoring can be done over hundreds of kilometers at a fraction of the cost of ground-survey-based monitoring.

9.4 Recommended Directions for Future Research.

Five research extensions are prioritised: (i) DEM Integration the coupling of Pleiades stereo-pair DEM (with ~1 m vertical accuracy) or UAV photogrammetry DSM with the 2D road mask, enabling full 3D highway parameter extraction (i.e., gradient, cross-fall, earthwork volumes); (ii) Lightweight CNN Hybridisation the addition of a binary road/non-road CNN classifier to the morphological pipeline, which requires only ~500 training patches and improves occlusion robustness without the need for full deep learning architecture; (iii) Multi-Temporal Construction Monitoring extension to (multi-temporal) satellite analysis, with bitemporal change detection and image co-registration to enable automated construction progress comparison to approved schedule; (iv) Network-Scale Automation batch-tile processing implementation on QGIS-tiled satellite imagery with OSM centreline priors to scale the single-segment approach to entire road networks; and (v) Standalone GUI Application compilation of the MATLAB pipeline as an executable desktop application with graphical user interface for non-specialist deployment at construction site offices.

Declarations

This research did not receive any funding from a public, commercial, or not-for-profit funding agency.

The authors report no conflicts of interest.

Ethics Clearance: Not relevant. This research included neither human participants nor animal subjects.

The authors encourage sharing their data for mutual benefit. Data availability statements often accompany research publications to clarify data availability and access.

REFERENCES

1. Buslaev, A., et al. (2018). Fully convolutional network for automatic road extraction from satellite imagery. In Proc. IEEE CVPRW, pp. 207–210.
2. Canny, J. (1986). A Computational Approach to Edge Detection. IEEE Transactions on Pattern Analysis and Machine Intelligence, 8(6), 679–698.
3. Chen, Z., et al. (2022). Road extraction in remote sensing data: A survey. ISPRS Journal of Photogrammetry and Remote Sensing, 183, 228–250.
4. Cheng, G., Wang, Y., Xu, S., Wang, H., Xiang, S., & Pan, C. (2017). Automatic Road Detection and Centerline Extraction via Cascaded End-to-End Convolutional Neural Network. IEEE Transactions on Geoscience and Remote Sensing, 55(6), 3322–3337.
5. Gao, L., Song, W., Dai, J., & Chen, Y. (2019). Road Extraction from High-Resolution Remote Sensing Imagery Using Refined Deep Residual Convolutional Neural Network. Remote Sensing, 11(5), 552.
6. Huang, X., & Zhang, L. (2012). Road Centerline Extraction from High-Resolution Imagery Based on Multiscale Structural Features and Support Vector Machines. International Journal of Remote Sensing, 33(5), 1523–1541.
7. Indian Roads Congress. (2018). IRC:37–2018: Guidelines for the Design of Flexible Pavements (4th Revision). Indian Roads Congress, New Delhi.
8. Indian Roads Congress. (2010). IRC:73–1980: Geometric Design Standards for Rural (Non-Urban) Highways (Reprint 2010). Indian Roads Congress, New Delhi.
9. Jia, Y., Zhang, X., Xiang, R., & Ge, Y. (2023). Super-Resolution Rural Road Extraction from Sentinel-2 Imagery Using a Spatial Relationship-Informed Network. Remote Sensing, 15(17), 4193.
10. Kaur, P., & Singh, A. (2019). GIS-Based Infrastructure Planning and Monitoring for Road Construction Projects. Journal of Infrastructure Systems (ASCE), 25(3), 04019019.
11. Lebaku, P. K. R., Gao, L., Lu, P., & Sun, J. (2024). Deep Learning for Pavement Condition Evaluation Using Satellite Imagery. Infrastructures, 9(9), 155.
12. Mena, J. B., & Malpica, J. A. (2003). An automatic method for road extraction in rural and semi-urban areas starting from high-resolution satellite imagery. Pattern Recognition Letters, 24(16), 3037–3058.
13. Mnih, V., & Hinton, G. E. (2010). Learning to detect roads in high-resolution aerial images. In Proc. ECCV, pp. 210–223.
14. Mokhtarzade, M., & Zoej, M. J. V. (2007). Road detection from high-resolution satellite images using morphological operators. International Journal of Applied Earth Observation and Geoinformation, 9(1), 32–40.
15. Mou, L., & Zhu, X. X. (2019). Vehicle instance segmentation from aerial image and video using a multi-task learning residual FCN. ISPRS Journal of Photogrammetry and Remote Sensing, 151, 3–13.
16. Ronneberger, O., Fischer, P., & Brox, T. (2015). U-Net: Convolutional Networks for Biomedical Image Segmentation. In Proc. MICCAI, Lecture Notes in Computer Science, vol. 9351, pp. 234–241. Springer, Cham.
17. Sghaier, M. O., Hammami, I., Foucher, S., & Labbé, M. (2018). Road Extraction from Very High Resolution Remote Sensing Optical Images Based on Texture Analysis and Beamlet Transform. IEEE Journal of Selected Topics in Applied Earth Observations and Remote Sensing, 11(5), 1459–1471.
18. Shamsudin, N., & Bindu, V. R. (2025). Extraction of Road from Super-Resolved Satellite Imagery using Semantic Segmentation. JISEM, 10(468), 285–291.
19. Xu, Q., Long, C., Yu, L., & Zhang, C. (2023). Road extraction with satellite images and partial road maps. arXiv:2303.12394.
20. Zhang, Z., Liu, Q., & Wang, Y. (2018). Road Extraction by Deep Residual U-Net. IEEE Geoscience and Remote Sensing Letters, 15(5), 749–753.
21. Ministry of Road Transport and Highways (MoRTH). (2023). Annual Report 2022–23. Government of India, New Delhi. Retrieved from https://morth.nic.in
22. Indian Roads Congress. (1983). IRC:86–1983: Geometric Design Standards for Urban Roads in Plains. Indian Roads Congress, New Delhi.
23. Indian Roads Congress. (2014). IRC:SP:84–2014: Manual of Specifications and Standards for Four Laning of Highways through Public Private Partnership. Indian Roads Congress, New Delhi.
24. National Highways Authority of India (NHAI). (2022). Bharatmala Pariyojana Phase I: Status Report. Ministry of Road Transport and Highways, New Delhi.
25. Otsu, N. (1979). A Threshold Selection Method from Gray-Level Histograms. IEEE Transactions on Systems, Man, and Cybernetics, 9(1), 62–66.
26. Gonzalez, R. C., & Woods, R. E. (2018). Digital Image Processing (4th ed.). Pearson Education, New York.
27. Heipke, C., Mayer, H., Wiedemann, C., & Jamet, O. (1997). Evaluation of automatic road extraction. International Archives of Photogrammetry and Remote Sensing, 32(3-2W3), 151–160.
28. Laptev, I., Mayer, H., Lindeberg, T., Eckstein, W., Steger, C., & Baumgartner, A. (2000). Automatic extraction of roads from aerial images based on scale space and snakes. Machine Vision and Applications, 12(1), 23–31.

29. Wiedemann, C., Heipke, C., Mayer, H., & Jamet, O. (1998). Empirical evaluation of automatically extracted road axes. Empirical Evaluation Methods in Computer Vision, 172–187.
30. Shi, W., Miao, Z., & Debayle, J. (2014). An integrated method for urban main-road centerline extraction from optical remotely sensed imagery. IEEE Transactions on Geoscience and Remote Sensing, 52(6), 3359–3372.
31. Hu, X., Li, Y., Shan, J., Zhang, J., & Zhang, Y. (2014). Road centerline extraction in complex urban scenes from LiDAR data based on multiple features. IEEE Transactions on Geoscience and Remote Sensing, 52(11), 7448–7456.
32. Hinton, G. E., Osindero, S., & Teh, Y. W. (2006). A fast learning algorithm for deep belief nets. Neural Computation, 18(7), 1527–1554.
33. He, K., Zhang, X., Ren, S., & Sun, J. (2016). Deep residual learning for image recognition. In Proc. IEEE CVPR, pp. 770–778.
34. Long, J., Shelhamer, E., & Darrell, T. (2015). Fully convolutional networks for semantic segmentation. In Proc. IEEE CVPR, pp. 3431–3440.
35. Demir, I., Koperski, K., Lindenbaum, D., Pang, G., Huang, J., Basu, S., & Raska, R. (2018). DeepGlobe 2018: A Challenge to Parse the Earth through Satellite Images. In Proc. IEEE CVPRW, pp. 172–181.
36. Van Etten, A., Lindenbaum, D., & Bacastow, T. M. (2018). SpaceNet: A Remote Sensing Dataset and Challenge Series. arXiv:1807.01232.
37. Mnih, V. (2013). Machine Learning for Aerial Image Labeling (Ph.D. Dissertation). University of Toronto, Toronto, Canada.
38. ESRI. (2020). ArcGIS Pro 2.7 Documentation: Remote Sensing and Image Analysis. Environmental Systems Research Institute, Redlands, CA.
39. Lillesand, T. M., Kiefer, R. W., & Chipman, J. W. (2015). Remote Sensing and Image Interpretation (7th ed.). John Wiley & Sons, Hoboken, NJ.
40. Richards, J. A., & Jia, X. (2006). Remote Sensing Digital Image Analysis: An Introduction (4th ed.). Springer, Berlin.
41. Bhatta, B. (2011). Remote Sensing and GIS (2nd ed.). Oxford University Press, New Delhi.
42. Gupta, R. P. (2018). Remote Sensing Geology (3rd ed.). Springer, Berlin.
43. Bureau of Indian Standards. (2002). IS:1200 (Parts 1–28): Methods of Measurement of Building and Civil Engineering Works. Bureau of Indian Standards, New Delhi.
44. Trimble Navigation Ltd. (2020). Trimble R8 GNSS System User Guide. Trimble Inc., Sunnyvale, CA.
45. QGIS Development Team. (2022). QGIS Geographic Information System, Version 3.28 LTS. Open Source Geospatial Foundation. Retrieved from https://qgis.org
46. MathWorks Inc. (2023). MATLAB R2023a Image Processing Toolbox User's Guide. MathWorks, Natick, MA.
47. Patra, S., Bhatt, U., & Ghosh, S. K. (2020). Road network extraction from high-resolution satellite imagery: A systematic review. Geocarto International, 35(15), 1707–1730.
48. National Remote Sensing Centre (NRSC). (2022). Cartosat-3 Satellite Data User Handbook. ISRO/NRSC, Hyderabad.
49. Pimpri-Chinchwad Municipal Corporation (PCMC). (2021). Development Plan 2041 for Pimpri-Chinchwad. PCMC, Pune.
50. Grün, A., & Li, H. (1995). Road extraction from aerial and satellite images by dynamic programming. ISPRS Journal of Photogrammetry and Remote Sensing, 50(4), 11–20.